Journal of Solid State Chemistry 182 (2009) 1649–1660

Contents lists available at ScienceDirect

Journal of Solid State Chemistry

journal homepage: www.elsevier.com/locate/jssc

Functionalized mesoporous materials for adsorption and release of different drug molecules: A comparative study

Gang Wang, Amy N. Otuonye, Elizabeth A. Blair, Kelley Denton, Zhimin Tao, Tewodros Asefa *

Department of Chemistry, 111 College Place, Syracuse University, Syracuse, New York 13244, USA

ARTICLE INFO

Article history:
Received 28 October 2008
Received in revised form
11 March 2009
Accepted 28 March 2009
Available online 9 April 2009

Keywords:
Drug delivery
Drug release
Drug adsorption
Nanostructured drug delivery vehicles
Functionalized mesoporous materials

ABSTRACT

The adsorption capacity and release properties of mesoporous materials for drug molecules can be improved by functionalizing their surfaces with judiciously chosen organic groups. Functionalized ordered mesoporous materials containing various types of organic groups via a co-condensation synthetic method from 15% organosilane and by post-grafting organosilanes onto a pre-made mesoporous silica were synthesized. Comparative studies of their adsorption and release properties for various model drug molecules were then conducted. Functional groups including 3-aminopropyl, 3-mercaptopropyl, vinyl, and secondary amine groups were used to functionalize the mesoporous materials while rhodamine 6G and ibuprofen were utilized to investigate the materials' relative adsorption and release properties. The self-assembly of the mesoporous materials was carried out in the presence of cetyltrimethylammonium bromide (CTAB) surfactant, which produced MCM-41 type materials with pore diameters of ~2.7–3.3 nm and moderate to high surface areas up to ~1000 m^2/g. The different functional groups introduced into the materials dictated their adsorption capacity and release properties. While mercaptopropyl and vinyl functionalized samples showed high adsorption capacity for rhodamine 6G, amine functionalized samples exhibited higher adsorption capacity for ibuprofen. While the diffusional release of ibuprofen was fitted on the Fickian diffusion model, the release of rhodamine 6G followed Super Case-II transport model.

1. Introduction

At present, the most common ways of delivering drugs to humans are oral administration and injection. However, these methods have lower efficiency for some therapies. Some therapeutic agents are unstable or poorly soluble drugs; therefore, new delivery systems are currently required. Functionalized nanostructured materials are increasingly considered as great candidates to make drug delivery vehicles and controlled drug release systems. This is because they have suitable platforms that can help minimize adverse reactions and unwanted side effects, that many conventional drugs used today often pose [1]. With some drug administration methods, the drugs have to often pass through various physiological obstacles before they reach their desired target, thus decreasing the amount of drug that gets to the targeted site. The inability to deliver controlled therapeutic concentration of drugs to the desired location can result in a decrease in the efficacy of the drug [1]. Increasing the concentrations of drugs to be delivered by using nanomaterial based drug delivery vehicles with improved adsorption capacity and controlled drug release properties can enhance the efficacy of the drugs.

Since their discovery in the early 1990s [2,3], a class of nanostructured materials called mesoporous silicates such as MCM-41 have attracted the attention of many scientists as drug delivery vehicles [4] because of their outstanding features such as high surface area (typically 1000 m^2/g), high porosity (typical pore volumes of 0.5–1.5 cm^3/g), well-ordered, tunable nanometer pores (typically 2–15 nm pore diameter) [5–7] and "non-cytotoxic" properties [8,9]. In fact, different types of mesoporous silica nanomaterials were already proved to be capable of carrying high dosages of a variety of drugs in their mesopores [4,10–12]. Additional benefits of mesoporous silica materials for drug delivery include the simplicity of tuning their pore sizes by changing their templates in order to better accommodate drug molecules of different sizes as demonstrated by extensive works by Vallet-Regí and co-workers [13] as well as other researchers [13,14]. While smaller drug molecules and biomolecules can be accommodated in mesoporous materials with smaller as well as bigger pore sizes, larger drug molecules require materials with bigger pore diameters [15]. Furthermore, mesoporous silica materials contain residual silanol groups, that can further be functionalized by different organic groups in order to modify their surface properties [16,17]. This creates favorable surface–drug interactions, which in turn result in improved adsorption capacity

* Corresponding author. Fax: +1 315 443 4070.
E-mail address: tasefa@syr.edu (T. Asefa).

0022-4596/$ - see front matter © 2009 Elsevier Inc. All rights reserved.
doi:10.1016/j.jssc.2009.03.034

of the materials for drug molecules. Lin and co-workers have shown that the organic functionalization of mesoporous materials can also influence their biocompatibility [18]. In addition to surface functional groups, the morphology and size of the mesoporous materials also have an important influence on drug release characteristics [19].

Generally, surface functionalization of mesoporous silica materials via covalent bonding of organic groups can be achieved by two methods: i.e., post-grafting synthesis [20] and co-condensation [20]. Although the post-grafting method results in well-ordered functionalized mesostructured materials, it often produces non-uniformly distributed organic groups because the organic moieties can congregate more on the channel pore mouth and on the exterior surfaces [21]. The Co-condensation synthetic method of mesoporous materials involves a one-step procedure and allows better control of the loading and distribution of the organic groups [22] although it often produces materials with less ordered mesoporous structures. In particular, low degree of structural integrity and long-range periodicity as well as lower surface area would be produced when the organosilane concentration in the synthesis exceeds ~25% [22].

Herein comparative investigations of the adsorption capacity and drug release properties of mesoporous materials whose surfaces are functionalized with judiciously chosen organic groups via post-grafting or co-condensation of various organosilanes were conducted. Furthermore, two different hydrophobic and hydrophilic molecules were used as model drugs in the study. The approach of organic functionalization of mesoporous materials for drug delivery has been considered previously [23–25]. The most studied system is ibuprofen adsorption on organic-functionalized matrices. When the MCM-41 or SBA-15 surface is functionalized with amino groups [23c,d], there is an ionic interaction between the carboxylate groups of ibuprofen and the ammonium groups on the matrix surface. The hydrophobicity of an ordered mesoporous silica can also be altered by modification of the surface with alkyl chains [23e]. As a result, the hydrophobic interaction with hydrophobic drugs can be improved. For instance, erythromycin release from functionalized matrices was much slower compared to unmodified material [23g]. Here a comparative study between grafting and co-condensation as well as the use of different functional groups and two different (model) drug molecules have been performed. Functional groups including 3-aminopropyl, 3-mercaptopropyl, vinyl, and secondary amine groups were used to functionalize the mesoporous materials while rhodamine 6G (R6G) and ibuprofen were used as probe molecules to investigate the materials' adsorption and release properties. The objectives of our study is to obtain the relative effect of functional groups as well as type of synthetic method to the functionalized materials on the adsorption and release properties of the materials for different molecules. The self-assembly of the mesoporous materials was carried out with cetyltrimethylammonium bromide (CTAB) surfactant producing MCM-41 type materials with pore diameters of ~2.7–3.3 nm and moderate to high surface areas up to ~1000 m^2/g. By changing the organic groups, the properties of the mesoporous materials were tuned from hydrophobic to hydrophilic and their adsorption and release properties for different (model) drug molecules such as rhodamine 6G and ibuprofen varied.

Rhodamine 6G and ibuprofen were chosen as probe molecules in our study because of their differences in hydrophilicity (or hydrophobicity), which allows the investigation of interaction of different molecules with functionalized mesoporous materials [24]. Furthermore, they are easy to probe by UV–Vis absorption spectroscopy. The solubility of rhodamine 6G and ibuprofen is dependent on solvent and pH of solution. For instance, the solubility of rhodamine 6G is 20 g/L in water; 40 g/L in butanol, 80 g/L in ethanol, 15 g/L in propanol and 100 g/L in diethylene glycol. Rhodamine 6G has increased solubility at higher pH [26]. Ibuprofen, which is a relatively weak acid with pka value of 4.4, has low solubility in water or at acidic pH. Ibuprofen has an intrinsic solubility of ~0.06 mg/mL in water. Ibuprofen is sparingly soluble in hexane and freely soluble in ethanol, octanol and dimethyl sulfoxide and chloroform with values of >10 g/L in acetone, >10 g/L in ethanol, 33 g/L in octanol, and 3.3 g/L in hexane. The solubility of ibuprofen increases sharply with pH, i.e. the drug is largely insoluble at low pH, but is readily soluble at alkaline pH. For example in water, its solubility is $\sim 0.5 \times 10^{-1}$ g/L at pH < 2.00 but $\sim 1 \times 10^{2}$ g/L at pH = 7.5 [27]. Based on these properties or because rhodamine 6G is quite soluble in water while ibuprofen is rather soluble in solvents such as hexane and ethanol, we have considered rhodamine 6G to be a hydrophilic probe molecule while ibuprofen is considered hydrophobic in this study. Therefore, they are expected to show different adsorption and release properties in organic functionalized mesoporous materials.

Our studies indicated that while the samples functionalized with mercaptopropyl and vinyl groups resulted in high adsorption capacity for rhodamine 6G, those functionalized with amine groups showed higher adsorption capacity for ibuprofen. Similarly, the drug release properties also varied from sample to sample, depending on the type of functional groups they contained. Furthermore, differences in adsorption capacity and drug release properties between the materials synthesized via co-condensation and those synthesized via post-grafting were also observed. The results of our study may give further insights into rational synthetic approaches to functionalized mesoporous materials with improved adsorption capacity and release properties for a variety of hydrophobic and hydrophilic drugs.

2. Experimental section

2.1. Materials and reagents

Tetraethoxysilane (TEOS), 3-aminopropyltriethoxysilane (APTS), rhodamine 6G, cetyltrimethyammonium bromide (CTAB), ibuprofen sodium salt, 3-mercaptopropyltrimethoxysilane (MPTS), vinyltrimethoxysilane (VTS), NaCl, $NaHCO_3$, KCl, $K_2HPO_4 \cdot 3H_2O$, $MgCl_2 \cdot 6H_2O$, $CaCl_2$, Na_2SO_4, $NH_2C(CH_2OH)_3$, and bis(triethoxysilylpropyl)amine (BTSPA) were obtained from Sigma-Aldrich. Hydrochloric acid (36.5%) and anhydrous toluene were purchased from Fisher Scientific.

2.2. Synthesis of functionalized mesoporous materials via co-condensation

A solution of 33.4 mL distilled water and 15 mL ammonium hydroxide was prepared and 2.30 mmol CTAB was dissolved in it by stirring. Then, a mixture of 17 mmol TEOS and 3.0 mmol of one of the organosilanes (MPTS, VTS, APTS, or BTSPA) was added. The solution was stirred at room temperature for 2 h and then stored in oven at 80 °C for two days. The sample was cooled down and filtered over Whatman-1 filter paper. The solid was washed thoroughly with large amount of distilled water and dried under ambient condition resulting in organic-functionalized mesostructured materials containing 3-mercaptopropyl, vinyl, 3-aminopropyl, or N,N-diproplyamine groups, respectively. The surfactant template was extracted by stirring 2 g of the functionalized mesostructured material with a solution of 50 mL methanol and 10 mL HCl for 5 h at 50 °C. The solution was filtered over a Whatman filter paper. The solid was washed three times with

20 mL methanol and dried under vacuum for 30 min. This resulted in organic-functionalized samples that were denoted as Co-MPTS, Co-VTS, Co-APTS, and Co-BPSPA, which contained 3-mercaptopropyl, vinyl, 3-aminopropyl, or N,N-diproplyamine groups, respectively.

2.3. Synthesis of functionalized mesoporous materials via post-grafting

First, mesoporous silica was prepared and then functionalized with different organic groups. Typically, a solution of 960 mL distilled water, 10.9 mmol CTAB and 40 mL NaOH (2.0 M) was prepared at 80 °C. The solution was stirred at 80 °C for 30 min. After adding 22.6 mL of TEOS, the solution was stirred for 2 h at 80 °C. It was then filtered over Whatman-1 filter paper and the solid was washed thoroughly with copious amount of distilled water, and dried under ambient condition. The surfactant template was extracted by stirring 1 g of the functionalized mesostructured material with a solution containing 150 mL ethanol and 0.6 mL HCl for 5 h at 50 °C to produce mesoporous silica, MCM-41. The extracted MCM-41 was grafted with 3-mercaptopropyl, vinyl, 3-aminopropyl, and secondary amine groups by stirring 600 mg MCM-41 with 4.4 mmol of MPTS, VTS, APTS, or BTSPA, respectively, in 100 mL toluene for 5 h. The samples were then washed with copious amount of ethanol and let to dry. The MCM-41 to organosilane ratio of 600 mg/4.4 mmol was chosen in order to ensure that excess organosilane is present in the solution. Many of our and others' previous studies [19] have shown that this ratio is optimum for obtaining the maximum possible grafted groups in the materials.

2.4. Adsorption of rhodamine 6G

Typically, a solution of 50 μM rhodamine 6G dye was prepared in distilled water at room temperature. Then, 100 mg of the the organic-functionalized mesoporous sample and 50 mL of the rhodamine 6G solution were mixed and stirred. Every 30 min, the solution was centrifuged for 5 min and then the supernatant was analyzed with UV–Vis absorption spectroscopy, by monitoring the major peak at 534 nm, which corresponds to the absorption maximum of rhodamine 6G. The absorption measurement was repeated, until the sample had stopped adsorbing more dye or until the absorption spectra of the supernatant had barely changed, indicating that saturation point was reached. Upon nearly complete adsorption of rhodamine 6G from the supernatant by the material, more rhodamine 6G solution was added into the sample and the above procedure was repeated.

In another experiment, 50 mg sample was kept in different concentrations of rhodamine 6G solutions for two days and after centrifugation, the absorbance of the supernatant was measured. This allowed us to plot % adsorption versus concentration, which allowed us to determine the adsorption capacity of the samples.

2.5. Release of rhodamine 6G

The experiments involving rhodamine 6G release by the samples were performed in a simulated body fluid (SBF) solution at 37 °C [16]. The SBF solution was prepared by mixing NaCl (0.14 mol), $NaHCO_3$ (4.20 mmol), KCl (3.00 mmol g), $K_2HPO_4 \cdot 3H_2O$ (1 mmol), $MgCl_2 \cdot 6H_2O$ (1.50 mmol), 1 N HCl (40 mL), $CaCl_2$ (2.50 mmol), Na_2SO_4 (0.50 mmol), and $NH_2C(CH_2OH)_3$ (49.90 mmol). A saturated sample with rhodamine 6G was first prepared by mixing 100 mg of the functionalized mesoporous samples with 50 mL volume of 50 μM of rhodamine 6G solution until the mesoporous sample had almost stopped adsorbing more rhodamine 6G, as monitored by UV–Vis absorption spectroscopy. The solution was filtered and the solid was washed with 20 mL of water. This washing procedure was used to remove excess rhodamine 6G molecules on the outer surface of the materials [24g]. The amount of rhodamine 6G on the external area was calculated to be 2.0–4.5% by subtracting the amount of rhodamine 6G removed in the washing steps from the total amount adsorbed initially. The total loading of rhodamine 6G in the mesoporous channels is calculated to be 30–55 mg for 100 mg material (Table 2). Then, 100 mg the rhodamine 6G saturated sample was mixed 50 mL SBF solution of pH 7.4 at 37 °C and stirred for 2 h. The solution was centrifuged for 5 min and then the UV–Vis absorption of 5 mL of the supernatant was tested by monitoring the absorption maximum of rhodamine 6G at 534 nm. The SBF/rhodamine 6G supernatant solution used for the measurement was discarded and the same volume of a fresh SBF solution was then added into the sample. After stirring and centrifugation of the solution, by following the same procedure above, the supernatant was analyzed again by UV–Vis spectroscopy. This experiment was repeated until the release of rhodamine 6G by the sample remained insignificant.

2.6. Adsorption of ibuprofen

With the same functionalized mesoporous materials, adsorption and release experiments with ibuprofen were performed. First, ibuprofen was prepared by stirring 4.4 mmol of commercially available ibuprofen sodium salt in 40 mL, 0.2 M HCl solution overnight at room temperature. The ibuprofen was let to crystallize. The solution was then filtered over Whatman-1 filter paper and the solid ibuprofen was dried under vacuum for 30 min. A solution of ibuprofen with a concentration of 2.2 mM in ethanol was prepared. The UV–Vis absorption experiments were carried out with this solution by following the procedure mentioned above for rhodamine 6G but by monitoring the absorption maximum of ibuprofen at 264 nm. To determine the % of adsorption of ibuprofen on the external surface of the materials, 50 mg of functionalized mesoporous sample was soaked in 50 mL of 24.2 mM ibuprofen solution for 24 h. It was then filtered and quickly washed once with 20 mL ethanol to remove excess ibuprofen coating on the outer surface of the materials [24g]. The amount of ibuprofen on the external area was calculated by subtracting the amount of ibuprofen removed in the washing steps from the total amount adsorbed initially.

2.7. Ibuprofen release experiments

Typically, 50 mg of the functionalized mesoporous sample that was saturated with ibuprofen above was stirred in 10 mL of SBF solution at pH 7.4 at 37 °C. After centrifugation of the sample for 5 min, 5 mL of the supernatant was tested with UV–Vis spectroscopy every 30–60 min to ensure that the mesoporous sample was saturated with ibuprofen. The release experiments were generally carried out by following the same procedure as the one carried out for rhodamine 6G above, except monitoring the absorption maximum of ibuprofen at 264 nm.

2.8. Characterization

The UV–Vis absorption spectra were measured with a Lambda-950 spectrophotometer (PerkinElmer). The thermogravimetric (TGA) traces were collected by using a Q-500 Quantachrome Analyzer (TA-Instruments) with N_2 (99.999%) as a carrier gas with a heating ramp of 5 °C/min. The low angle powder X-ray diffraction (XRD) patterns were obtained with a Scintag

Diffractometer. The BET gas adsorption–desorption measurements were done with Micromeritics Tristar 3000 volumetric adsorption analyzer, after degassing the samples at 160 °C for 12 h. The solid-state ^{13}C (75.5 MHz) and ^{29}Si (59.6 MHz) NMR spectra were acquired on a Bruker AVANCE 300 NMR spectrometer. For ^{13}C CP-MAS NMR experiments, 7.0 kHz spin rate, 5 s recycle delay, 1 ms contact time, $\pi/2$ pulse width of 5.6 μs, and 600 scans using TPPM ^{1}H decoupling were employed. For the ^{29}Si CP-MAS NMR experiments, 7.0 kHz spin rate, 10 s recycle delay, 10 ms contact time, $\pi/2$ pulse width of 5.6 μs, and 600 scans by using TPPM ^{1}H decoupling were employed.

3. Results and discussion

3.1. Synthesis and characterization of functionalized mesoporous materials

The X-ray diffraction patterns of the functionalized mesoporous materials and representative TEM images of samples synthesized by post-grafting and co-condensation are shown in Fig. 1. The X-ray diffraction patterns of all the samples synthesized by post-grafting exhibited hexagonally ordered mesoporous structure that is characteristic of MCM-41-type materials (Fig. 1, I). The X-ray diffraction patterns (Fig. 1B) of the samples synthesized by co-condensation from VTS and MPTS (Co-VTS and Co-MPTS) also showed ordered mesostructures; however, those synthesized from APTS (Co-APTS) and BTSPA (Co-BTSPA) revealed less ordered mesostructures. The weakly ordered mesostructure in the latter is probably a result of the fact that hydrophilic organoamine groups in APTS and BTSPA cause some perturbation in the center or the hydrophobic core of the surfactant micelles during co-condensation synthesis of mesostructured materials from these organosilanes [28]. From the (100) Bragg peak, the *d*-spacing values of both Co-VTS and Co-MPTS samples as well as those synthesized by post-grafting were calculated to be ~4.3–4.5 nm. Furthemore, except for a slight decrease in their (100) Bragg reflection, the samples remained mesostructured with the same unit cell size after adsorption and release of rhodamine 6G and ibuprofen guest molecules (Fig. 1, II). The decrease in the intensity of Bragg reflection is probably a result of a slight decrease in electron contrast between the mesopores and the mesopore channel walls due to the confinement of the R6G and ibuprofen guest molecules inside the mesopores [17]. Although the unit cells remained the same, the pore diameters and surface areas of the materials decreased after adsorption of the drug or guest molecules.

The morphology and mesopores of the materials are shown in Fig. 1, III. Although the morphology and size of the mesoporous materials are known to have an important influence on drug release characteristics [29,30], the materials we used for our comparative studies are made from the same batch of parent material, and consequently had similar morphologies. This is, therefore, expected to cause little difference on the adsorption and release properties of the materials in our studies.

The structures of the functionalized samples were also characterized by nitrogen gas adsorption. The gas adsorption (Fig. 2) showed a type IV isotherm with sharp capillary condensation steps for all the samples synthesized by post-grafting as well as for samples Co-MPTS and Co-VTS that were synthesized by co-condensation. This is indicative of the presence of mesoporous structure in these materials. This result is also consistent with their XRD patterns shown in Fig. 1. The specific surface area and pore sizes of the materials are reported in Table 1. It is worth noting that all the samples synthesized by post-grafting and the samples synthesized by co-condensation from VTS and MPTS showed high surface areas. The samples synthesized from APTS and BTSPA by co-condensation showed significantly lower surface areas. The pore size distributions of the materials are shown in Fig. 3 and their average mesoporous diameters are listed in Table 1. It is important to note here that the absolute values of the pore diameters have to be treated with caution as the BJH method, in general, underestimates the pore diameter of mesoporous materials [31]. We also calculated corrected values of pore diameters by using the equation developed by Kruk and Jaroniec [31a,c]. The results reveal that the materials synthesized by post-grafting have average mesopore diameters between 2.7–3.2 nm while the samples synthesized by co-condensation have average mesopore diameters of 3.0–3.3 nm (Table 1). The average pore diameters of samples Co-VTS and Co-MPTS were slightly lower than the corresponding samples synthesized by post-grafting. This is consistent with previously reported materials from co-condensation of hydrophobic organosilanes, which showed smaller pore sizes and whose pore sizes depend on the relative concentration of the organonosilane in the solution [32]. Furthermore, upon immobilization of the guest or drug molecules, the surface areas of the materials decreased. For instance, the surface area of the Co-MPTS sample decreased from 885 to 352 m^2/g after getting saturated with rhodamine 6G.

Typical ^{29}Si CP-MAS NMR spectra for the functionalized samples are shown in Supplementary materials (Fig. S1). The spectra showed peaks at around −100 and −110 ppm which correspond to hydroxyl containing silicon sites (Q^3 or $SiO_{1.5}OH$) and cross-linked silicon (Q^4 or SiO_2), respectively. The spectra also exhibited peaks between −50 and −80 ppm that were assigned to the Si atoms covalently bonded to organic groups or T^2 [$(SiO)_2Si(OH)(CH_2–)$] and T^3 [$(SiO)_3Si(CH_2)$] sites [25]. The ^{13}C CP-MAS NMR spectra (Fig. S2) of APTS and MPTS functionalized samples showed a signal at ~10 ppm, which was assigned to methylene, $–CH_2–$, groups that are directly bonded to silicon atom. The resonances between 20 and 30 ppm were attributed to the other methylene and the terminal methyl groups of the propyl chain [33]. Furthermore, Figs. S2,B, S2,C, and S2,D showed additional minor peaks at ~30 ppm that were assigned to carbon atoms of residual CTAB surfactant in the pores of the samples. These peaks were observed in the spectra for samples grafted with MPTS, VTS and BTSPA while they were not visible on the spectrum for the sample grafted with APTS (Fig. S1,A) although all these four samples were prepared from the same batch of surfactant-extracted MCM-41. This is because the density of organic groups grafted in the former three samples was significantly lower than that in the APTS-grafted sample. Thus, the residual surfactant peaks appeared more visible with respect to the peaks corresponding to the organic functional groups in the former than in the latter.

The mesoporous materials were further characterized by thermogravimetric analysis under nitrogen (Table S1 and Fig. S3) and elemental analysis (Table 2). These results further corroborated the results obtained from solid-state NMR. Thermogravimetric analysis of organic functionalized mesoporous materials under nitrogen or air were previously used by many groups for characterization of organic functionalized mesoporous materials [34]. The TGA traces of the functionalized samples (Fig. S3) showed a weight loss below 100 °C due to physisorbed water [35] and, most importantly, a weight reduction between ~200 and 600 °C due to the loss of organic functional groups. Furthermore, a slight weight reduction after 600 °C due to loss of water molecules from condensation of residual silanols was observed. Elemental analysis revealed that the mmol organic/g of sample synthesized by post-grafting of APTS, BTSPA, MPTS, and VTS were 2.17, 0.94, 0.97, and 1.53 mmol/g, respectively (Table 2).

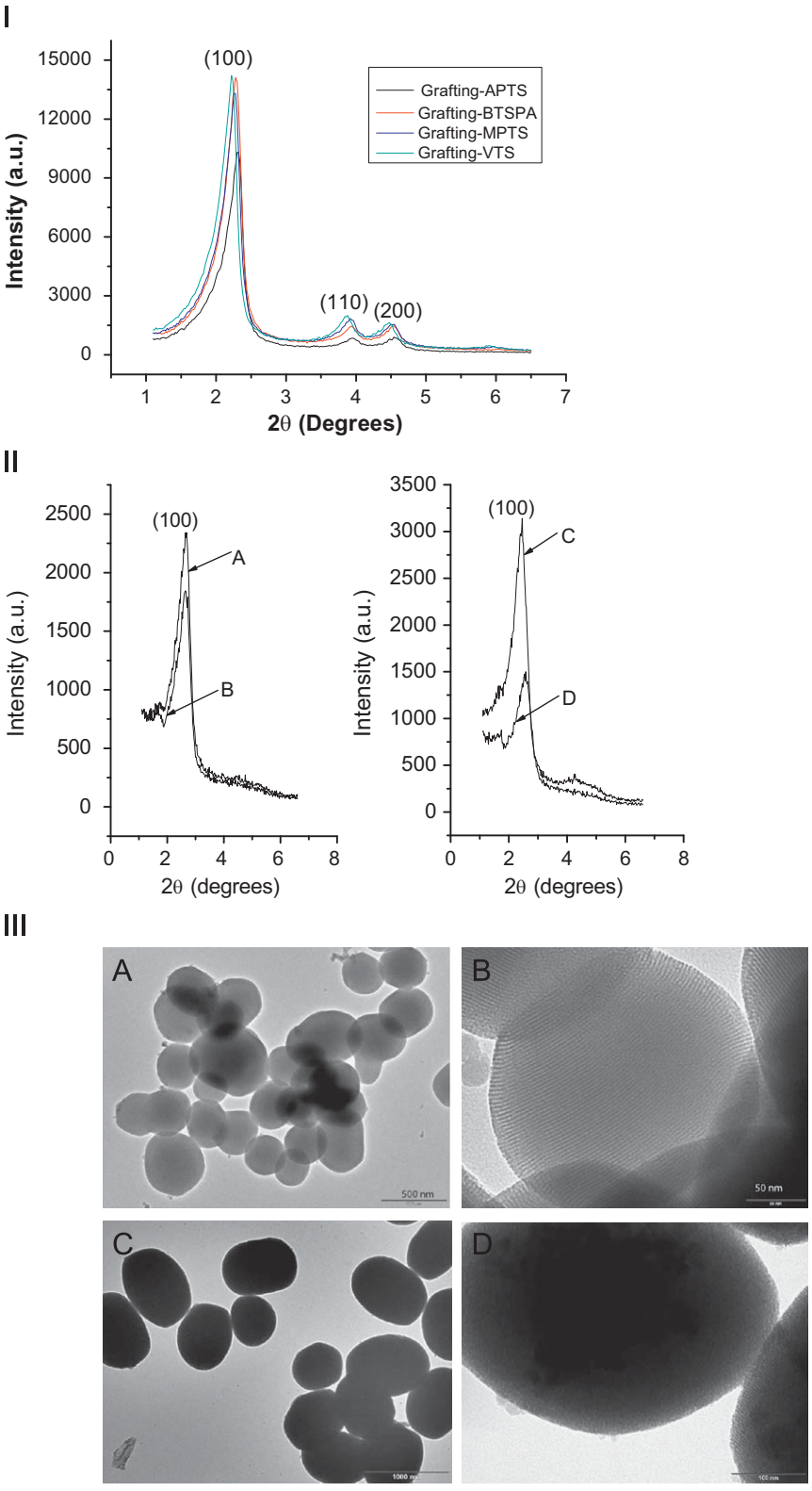

Fig. 1. (I) Powder X-ray diffraction (XRD) patterns of functionalized mesoporous samples synthesized by post-grafting of organosilanes MPTS, VTS, APTS and BTSPA onto mesoporous silica. (II) Powder X-ray diffraction (XRD) patterns of functionalized mesoporous samples synthesized by co-condensation of organosilanes (A) MPTS and (C) VTS with the corresponding XRD patterns of the samples after R6G adsorption shown in (B) and (D), respectively. (III) Low resolution and high resolution TEM Images of mesoporous samples synthesized by (A,B) post-grafting and (C,D) co-condensation.

This indicated that the surface density of functional groups that were grafted decreased in the order of APTS > VTS > MPTS ≅ BTSPA. On the other hand, the mmol organic/g sample in the samples synthesized by co-condensation, Co-MPTS and Co-VTS, were 2.18 and 2.57 mmol/g, respectively (Table 2). This indicates that the mmol of functional groups in the samples is higher for sample prepared from VTS than that from MPTS (or Co-VTS > Co-MPTS). We can also conclude from Table 2 that

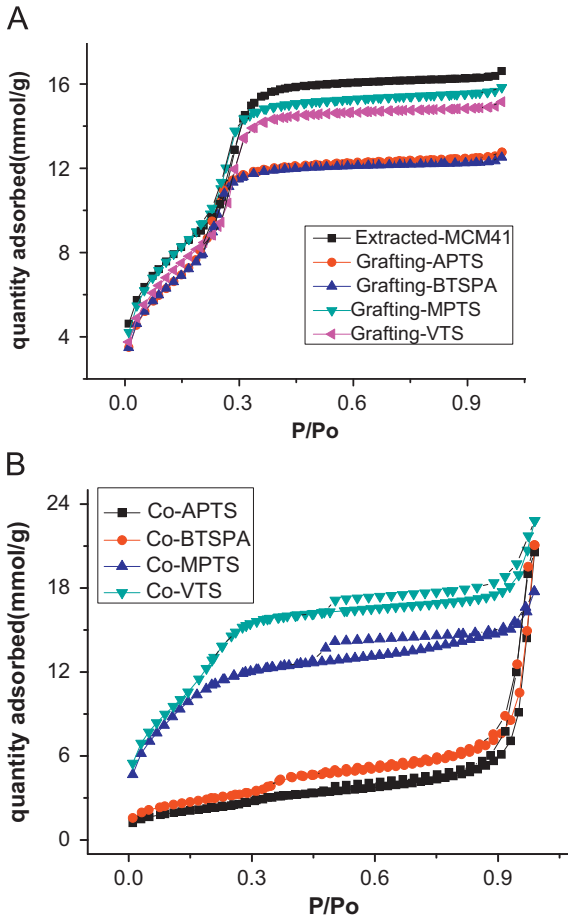

Fig. 2. Nitrogen adsorption isotherms of samples synthesized by (A) post-grafting and (B) co-condensation of different organosilanes.

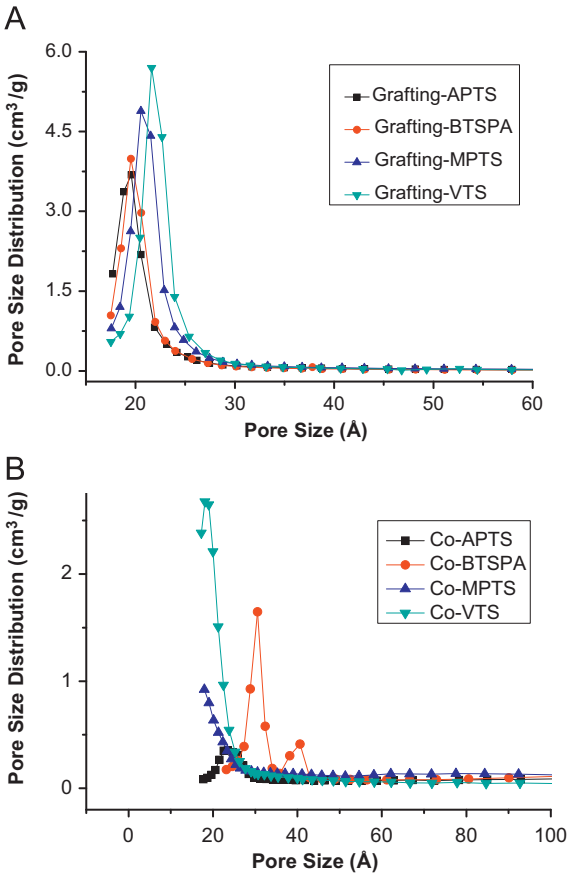

Fig. 3. Pore size distribution of functionalized samples synthesized by (A) post-grafting APTS, BTSPA, MPTS, and VTS, onto MCM-41 and (B) co-condensation of APTS, BTSPA, MPTS, and VTS with TEOS.

Table 1
Structural data of organic functionalized mesoporous materials.

Samples	Surface area (m^2/g)	Average BJH mesopore diameter (Å)[a]	Average mesopore diameter by KJS method (Å)[b]
Co-APTS	189	2.4	3.1
Co-BTSPA	238	2.3	3.2
Co-MPTS	885	2.2	2.7
Co-VTS	1183	2.4	3.0
Grafting-APTS	887	2.0	3.0
Grafting-BTSPA	852	2.0	3.0
Grafting-MPTS	952	2.1	3.2
Grafting-VTS	811	2.2	3.3

[a] The pore diameters were obtained by the BJH method, which is known to underestimate the pore diameter of mesoporous materials (see Ref. [31]). It is, therefore, worth noting that the absolute values of these pore diameters have to be treated with caution.

[b] The pore diameters were calculated by an equation developed by Kruk and Jaroniec [31a,c].

the sample synthesized from MPTS and VTS by co-condensation had more functional groups compared to the corresponding sample synthesized by post-grafting.

3.2. Adsorption and release of rhodamine 6G

By using the Beer–Lambert law, the amount of molecules adsorbed in the mesoporous samples or released by the samples was calculated. Although there was no significant difference in surface area and pore size (Table 1) between the four samples synthesized by post-grafting, the samples functionalized with vinyl and mercaptopropyl groups adsorbed significantly more rhodamine 6G than the samples functionalized with primary and secondary amines (Table 2 and Fig. 4). This trend was also true for samples synthesized by co-condensation. Upon comparing samples synthesized under similar conditions, the samples containing mercaptopropyl groups were found to adsorb the most rhodamine 6G than the sample containing vinyl groups, which in turn adsorbed more than the amine-functionalized sample (Table 2). Generally, the adsorption capacity values for rhodamine 6G appeared to be the highest in the sample containing mercaptopropyl groups than vinyl groups and in samples synthesized by co-condensation than by post-grafting (Table 2). The adsorption capacity of the amine functionalized samples for rhodamine 6G was significantly lower. Careful analysis of the adsorption capacities by normalizing them with respect to the density of functional groups in the materials as well as their surface areas were conducted (Table 2). It indicated that the samples containing mercaptopropyl groups with grafting and co-condensation synthesis gave values of 1.5×10^{-4} and 3.3×10^{-4} mmol/m^2, respectively, while those containing vinyl groups with grafting and co-condensation gave 4.9×10^{-5} and 6.8×10^{-5} mmol/m^2, respectively. The samples synthesized from APTS and BTSPA by grafting gave values of 1.1×10^{-7} and 2.3×10^{-7} mmol/m^2, respectively. This indicates that the mercaptopropyl groups results in an order of magnitude higher adsorption capacity than those containing vinyl groups, which in

Table 2
Density of grafted organic groups (mmol/g) of functionalized mesoporous materials determined from elemental analysis and adsorption capacity of the samples for rhodamine 6G.

Samples	Grafting APTS	Grafting BTSPA	Grafting MPTS	Grafting VTS[a]	Co-MPTS	Co-VTS[a]
mmol R6G adsorbed/g sample	1×10^{-4}	2×10^{-4}	0.14	0.04	0.29	0.08
mmol Organic groups/g sample[b]	2.17	0.94	0.97	1.53	2.18	2.57
Average number of adsorbed molecules per one surface ligand	4.6×10^{-5}	2.1×10^{-4}	1.4×10^{-1}	2.6×10^{-2}	1.3×10^{-2}	3.1×10^{-4}
Normalized with surface area (mmol R6G adsorbed/surface area, mmol/m^2)	1.1×10^{-7}	2.3×10^{-7}	1.5×10^{-4}	4.9×10^{-5}	3.3×10^{-4}	6.8×10^{-5}

[a] mmol/g the samples functionalized with VTS could be slightly off as they were calculated based on the wt% of C and as the samples have some additional carbon from the residual surfactant.
[b] Determined from elemental analysis.

turn showed two orders of magnitude higher than the amine functionalized samples. The rate of adsorption seems to be very similar in all the samples in the initial period (for ~11 h). The samples functionalized with VTS by post-grafting as well as by co-condensation almost got saturated within the first 11 h. However, the samples functionalized with MPTS continued to adsorb more rhodamine 6G for more than 11 h.

The adsorption profiles plotted by measuring adsorption versus concentration are shown in Fig. 4C. All the lines were fit into one type of function, $Y = A(1-e^{-bX})$, where A and b are constants (Table 3). The term A represents the maximum drug adsorption by the materials while the value of (bA) represents the initial adsorption rate of the drug by the nanoparticles and the term (bAe^{-bX}) indicates that the adsorption rate decreases over time. Analysis of these terms A and b indicates that MPTS-functionalized samples have higher adsorption capacity than their corresponding VTS-functionalized samples in both cases, i.e. samples synthesized by grafting and co-condensation. Furthermore, the data shows that the initial adsorption rates of the samples decrease in the order of Co-MPTS > Grafting-MPTS > Co-VTS = Grafting-VTS.

The adsorption results shown in Fig. 4 were further complimented by comparing the weight losses between ~150 and 700 °C on thermogravimetric analysis (TGA) of the samples before and after adsorption of R6G. The weight loss between 150 and 700 °C can correspond to the decomposition of R6G or drug molecules. Fig. 5 shows the TGA traces of the samples after incubation in 50 μM R6G solution (or the samples shown in Fig. 4D). The TGA traces of sample Co-MPTS exhibited a 15.2% weight loss before adsorption of R6G adsorption and a 23.4% weight loss after adsorption of R6G (Fig. 5I). This corresponds to adsorbed R6G weight of 8.2% and consistent with the adsorption capacity obtained in the adsorption profile in Fig. 4D. The TGA traces of sample Co-VTS exhibited a 5.1% weight loss before rhodamine 6G adsorption and a 10.0% weight loss after R6G adsorption (Fig. 5II). This corresponds to R6G weight of 4.9%, which is also consistent with the adsorption capacity the sample obtained in Fig. 4D. The increase in the values of weight loss after adsorption of R6G clearly suggests that R6G was adsorbed in the samples and the difference between the two values corresponds to the amount of R6G adsorbed. These data indicate again that Co-MPTS adsorbed more R6G than Co-VTS and is consistent with the data obtained from the UV–Vis spectra analysis.

The difference in the degree of adsorption of R6G by the samples can aso be clearly seen by simply looking at the color of the mesoporous materials after treatment with R6G solution (Figs. 5D and E). After mixing the same mass mesoporous materials with the same volume and concentration of R6G solution for several hours and then separating the solid from the supernatant, samples with colors ranging from white to dark pink were obtained. While the samples functionalized with APTS and BTSPA almost still looked white, those functionalized with MPTS and VTS appeared deep pink colored. This indicates that the samples functionalized with APTS and BTSPA either by post-grafting or co-condensation adsorbed little rhodamine 6G while the samples functionalized with MPTS and VTS by both methods adsorbed greater amounts of R6G.

Comparison of the density of functional groups in the materials with respect to their adsorption properties to R6G reveals an interesting trend. Although the density of grafted groups in APTS functionalized sample is higher than that in the MPTS functionalized sample, the former has a lower degree of adsorption of R6G. The adsorption capacity of the samples was normalized with the density of organic functional groups in the materials and their surface areas. It reveals that the differences in adsorption properties of the samples to rhodamine 6G could be partially attributed to the differences in the type of the functional groups and possible degree of interaction between the functional groups and R6G molecules. Recently Suh et al. [23a] have made extensive studies in this area, which indicated that rhodamine based dyes with positive charges such as rhodamine 6G and rhodamine 123 show faster uptake than those with negative charged such as rhodamine 101. Their results suggested that the molecular charge of the drug has an important effect for the uptake rate of the drugs in the materials. This molecular-charge effect is the result of negative charges that are developed in the pore surfaces by the ionization of silanol groups in aqueous solution and their interactions with the charges of the incoming dye molecules. Among the positively charged dyes, both the molecular weight and the magnitude of the dipole moment seem to contribute to the diffusion kinetics of the dyes. Their study and Sekine and Nakatani [23f] have also reported uptake half-lives of 10–30 min at room temperature depending on the solution pH, the ionic strength, the type of material (powder versus thin film) as well as the channel length and pore structures. We observed that the uptake half-times are slightly longer than what was observed by others, with the MPTS-functionalized samples reaching to uptake half-lives more slowly than the VTS-functionalized samples. However, the former gave higher overall uptake of rhodamine 6G than the corresponding VTS-functionalized sample. Generally, the MPTS- and VTS-functionalized samples gave higher adsorption capacity than MCM-41 and amine-functionalized samples. The functional groups such as mercaptopropyl and vinyl, which are hydrophobic, favorably interact with the hydrophobic parts of rhodamine 6G, producing higher adsorption capacity to R6G compared to MCM-41 and the materials functionalized with organoamines. It appears that the hydrophilic organoamines, $-NH_2$ and –NH– groups, in the APTS and BTSPA functionalized materials, respectively, produce unfavorable interaction with the aromatic and alkyl chains of rhodamine 6G molecule and thus, result in lower adsorption capacity to R6G. In fact, the amine functional groups would likely to be protonated by abstracting a proton from the silanol groups [36]. This then leads to samples that have a positively charged

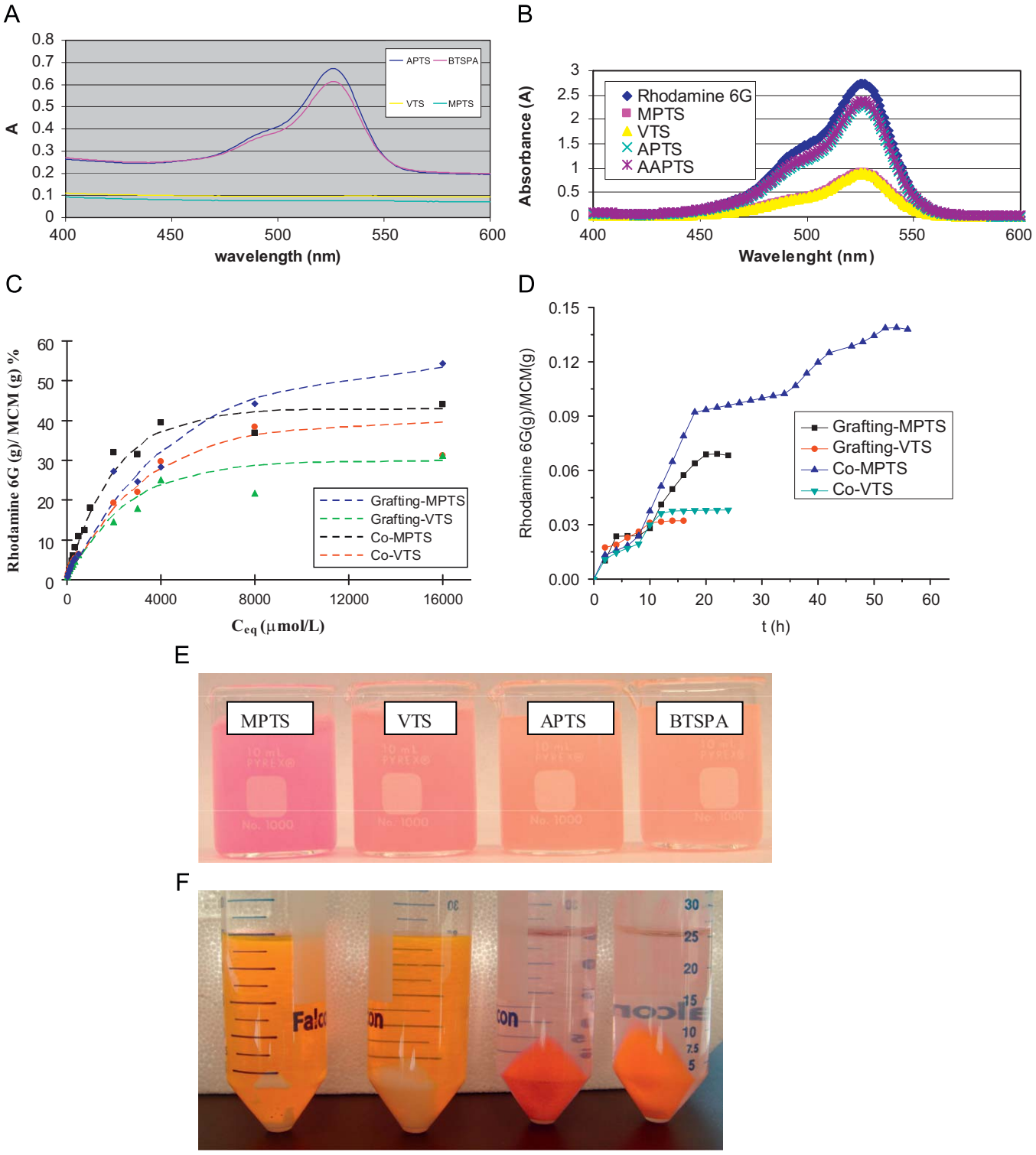

Fig. 4. Adsorption properties of rhodamine 6G in various functionalized mesoporous materials. (A) UV–Vis absorption spectra of R6G in the supernatant 20 min after adsorption of a solution of R6G with different functionalized mesoporous materials synthesized via co-condensation. (B) UV–Vis absorption spectra of R6G in the supernatant 20 min after adsorption of R6G with different functionalized materials that were synthesized via post-grafting. (C) Adsorption versus concentration of R6G for samples synthesized by post-grafting and co-condensation. (D) Percent of R6G adsorbed versus time profile of different samples synthesized by post-grafting and co-condensation using aqueous 50 μM rhodamine 6G solution. (E) Digital images showing colors of the functionalized mesoporous samples synthesized by co-condensation after adsorption of R6G. A bright color was observed for MPTS functionalized sample indicating that it has adsorbed the most R6G. (F) Digital images showing colors of the functionalized mesoporous samples synthesized by post-grafting after adsorption of R6G.

surface which is not conducive for adsorption of positively charged R6G molecules.

The trend in the degree of R6G release (Fig. 6) by the functionalized samples was found to be the reverse of the one observed for adsorption. The studies of R6G release were conducted in a simulated body fluid solution of pH of 7.40 at 37 °C [16]. SBF solution was chosen as it has similar composition as what is in our body and as it helps understanding how drug

Table 3
Values of terms A and b in the graphs for adsorption versus concentration of rhodamine 6G that are fit into a function: $Y = A(1-e^{-bX})$, where A and b are constants for each specific adsorption.

Particles	A (%)[a]	b (μmol^{-1}L)[b]	r^2
Co-MPTS	43	5×10^{-4}	0.98
Co-VTS	40	3×10^{-4}	0.99
Grafting-MPTS	55	2×10^{-4}	0.98
Grafting-VTS	30	4×10^{-4}	0.99

[a] The term A represents the maximum drug adsorption by the materials.
[b] The term (bA) indicates the initial adsorption rate of the drug by the nanoparticles while the value of (bAe^{-bX}) indicates that the adsorption rate decreases over time.

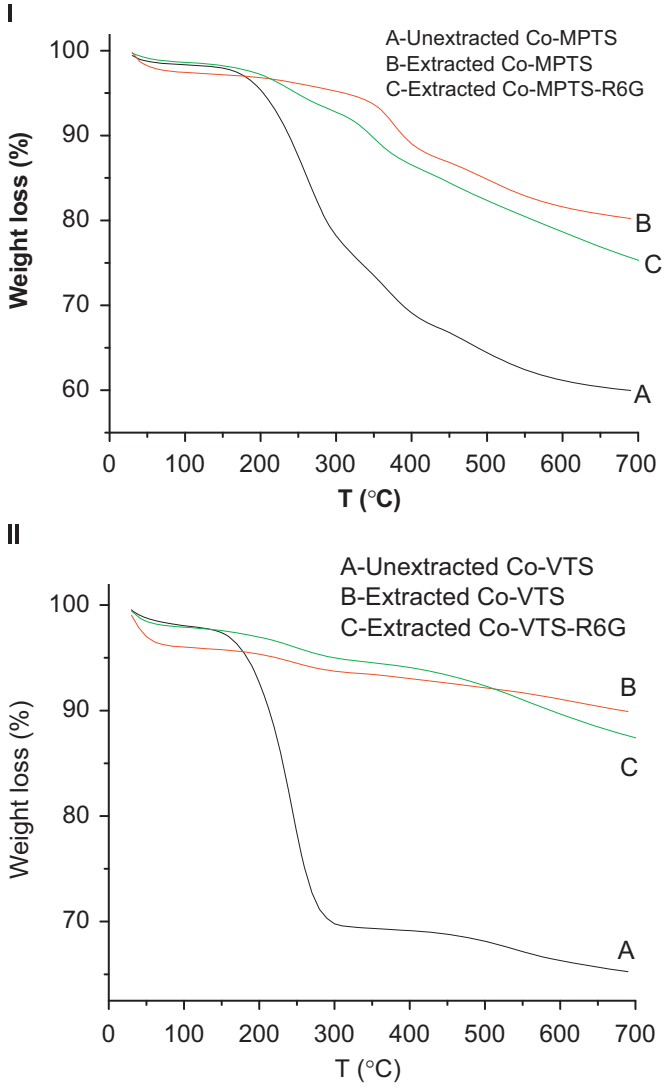

Fig. 5. Thermogravimetric (TGA) traces of before surfactant extraction (A), after surfactant extraction (B), and after R6G adsorption (C) for (I) samples synthesized by co-condensation of MPTS and (II) samples synthesized by co-condensation of VTS.

release properties of the materials would be in our body. The samples functionalized with VTS by post-grafting method released R6G molecules faster than the corresponding sample synthesized by co-condensation. On the other hand, the sample synthesized by post-grafting with MPTS released R6G molecules faster than the corresponding sample synthesized by co-condensation, therefore, the samples functionalized with VTS

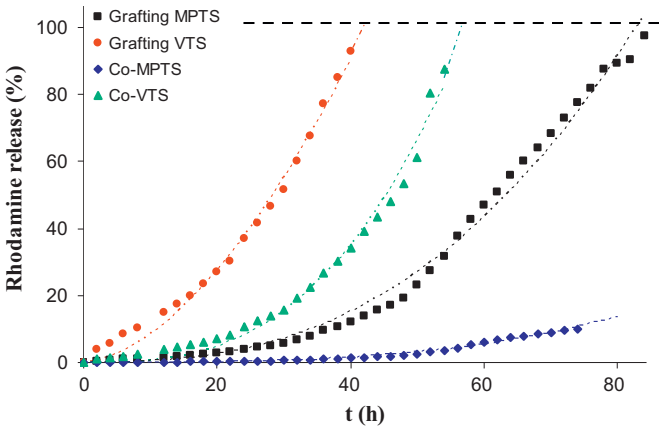

Fig. 6. Comparative release profiles percent of R6G released for different samples synthesized by post-grafting and co-condensation of MPTS and VTS. The graphs were fitted as function $Y = at^n$, where Y is % Release and t is time. This indicated that for samples grafted with MPTS, $a = 0.0011$, $n = 2.6$, $r^2 = 0.991$; grafted with VTS, $a = 0.16$, $n = 1.7$, $r^2 = 0.991$; sample Co-MPTS, $a = 1.14\times10^{-5}$, $n = 3.2$, $r^2 = 0.990$; and sample Co-VTS, $a = 9.1\times10^{-4}$, $n = 2.9$, $r^2 = 0.987$.

released R6G faster than the corresponding samples functionalized with MPTS.

The diffusional R6G release data was fitted onto a non-Fickian or a Super Case-II transport model [37,38] and followed diffusional release process that follow Eq. (1) below with $n > 1$:

$$Y = at^n \quad (1)$$

where Y is % Release and t is time. Further analysis of the data and the graph in Fig. 6 gave values of $a = 0.0011$, $n = 2.6$, $r^2 = 0.991$ for sample grafted with MPTS; $a = 0.16$, $n = 1.7$, $r^2 = 0.991$ for sample grafted with VTS; $a = 1.14\times10^{-5}$, $n = 3.2$, $r^2 = 0.990$ for sample Co-MPTS synthesized by co-condensation; and $a = 9.1\times10^{-4}$, $n = 2.9$, $r^2 = 0.987$ for sample Co-VTS synthesized by co-condensation.

3.3. Adsorption and release studies for ibuprofen

The adsorption experiments with ibuprofen (Fig. 7) exhibited a totally different trend compared to the results obtained for adsorption of R6G for the same series of samples. The UV–Vis absorption data showed that the samples functionalized with APTS and BTSPA by post-grafting had much more adsorption capacity for ibuprofen than for R6G. Furthermore, the sample grafted with APTS showed higher adsorption capacity of ibuprofen than the corresponding sample grafted with BTSPA (Fig. 7A). On the other hand, the samples synthesized from MPTS and VTS, either by co-condensation or grafting, and the parent MCM-41 showed almost no adsorption of ibuprofen (Figures not shown). The UV–Vis absorption results were corroborated by TGA data (Table 4 and Fig. 7B). These results are interesting considering the fact that elemental analysis (Table 2) shows the BTSPA-grafted sample has almost similar mmol of grafted groups as the MPTS-grafted sample but much less than the VTS-grafted sample and the APTS-grafted sample has less mmol of functional groups than the VTS-grafted sample. This further indicates that the type of functional groups (or the degree of their interaction with ibuprofen) and not their density in the materials is mainly responsible for the differences in adsorption capacity of materials. Since ibuprofen contains a carboxylic acid group, these carboxylic acid groups could interact favorably with the $-NH_2$ and $-NH-$ groups in the amine-functionalized samples via hydrogen bonding, producing higher adsorption capacity of these samples for ibuprofen. On the other hand, the hydrophobic mercaptopropyl and

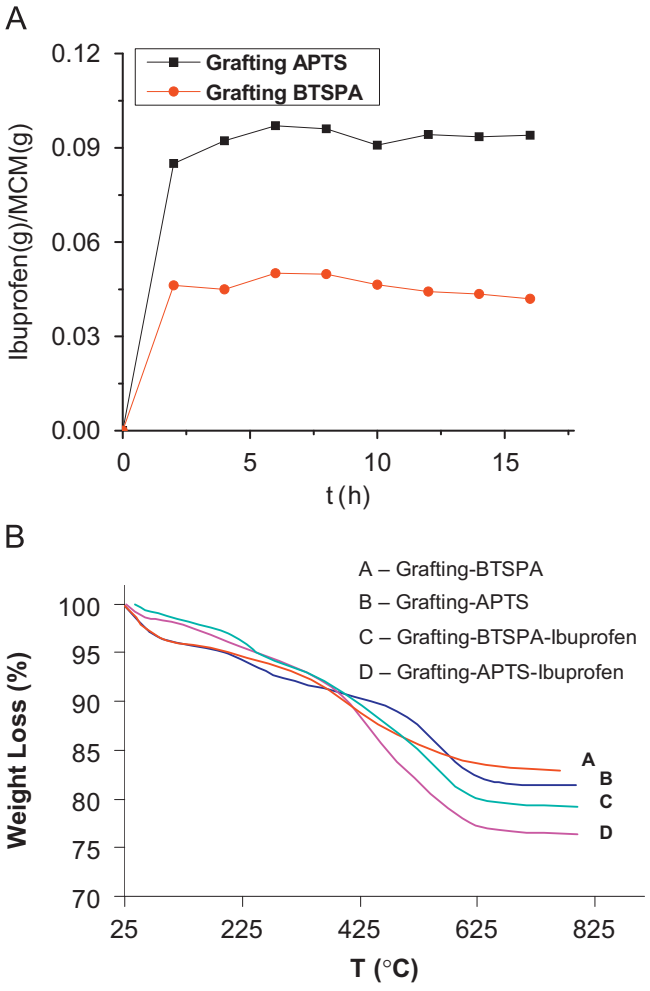

Fig. 7. Adsorption properties of ibuprofen by various amine functionalized mesoporous materials. (A) Percent of ibuprofen adsorbed versus time profile of samples synthesized by post-grafting. (B) Thermogravimetric analysis of mesoporous materials before and after adsorption of ibuprofen.

Table 4
Percent weight loss between 200 and 600 °C for samples grafted with APTS and BTSPA, before and after adsorption of ibuprofen.

Samples	Before adsorption (%)	After ibuprofen adsorption (%)
Grafting APTS	11.8	18.0
Grafting BTSPA	11.0	16.2

vinyl groups in VTS and MPTS functionalized samples, respectively, have unfavorable interaction with ibuprofen, producing less adsorption capacity for ibuprofen. These results are consistent with those reported by others for similar functional groups [37].

The % of adsorption of ibuprofen coating on the outer surface of the materials was obtained by soaking the samples in ibuprofen solution, then filtering and quickly washing the materials once with 20 mL ethanol [24g]. The value was found to be 3.6 and 9.8% for the APTS and BTSPA functionalized samples, respectively. The corresponding total loading of ibuprofen in 50 mg samples were 30.2 and 33.2 mg, respectively.

The rate of drug release of ibuprofen by the samples functionalized with APTS and BTSPA were found to be essentially similar (Fig. 8). The diffusional release data for ibuprofen followed a Fickian diffusion process and it was fitted on the Higuchi equation ($Y = at^n$) [38–40], where Y is % Release, t is time, and k

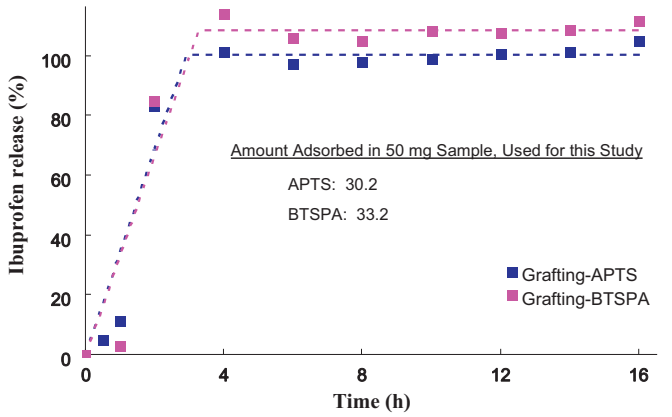

Fig. 8. (A) Release of ibuprofen in SBF solution by different samples functionalized with APTS and BTSPA. The graph for sample grafting APTS was fitted as $Y = kt^{1/2}$ ($t < 2.6$), $Y = 100$ ($t > 2.6$), $r^2 = 0.996$ and the graph for sample grafting BTSPA was fitted as $Y = kt^{1/2}$ ($t < 2.6$), $Y = \sim 100$ ($t > 2.6$), $r^2 = 0.996$.

Table 5
Date of ibuprofen release shown in Fig. 8 for APTS and BTSPA grafted samples after the graphs are $Y = kt$ (if $t < t^*$) or $Y = A$ (if $t \geq t^*$), where Y represents percentage of ibuprofen released, and t is time.

Samples	k (h^{-1})	t^* (h)	A (%)	r^2
Grafting-APTS	34.2	2.9	100.3	0.95
Grafting-BTSPA	32.9	3.3	108.6	0.94

t^* is a time constant when the release reaches equilibrium (A, i.e., the maximum release), whereas k stands for the rate at which ibuprofen gets released by the materials.

stands for the rate at which ibuprofen gets released by the particles. After peak fitting the data, we obtained $n = 1$ for $t < t^*$, where t^* is a time constant when the release reaches equilibrium (A, i.e., the maximum release), and has values of 2.9 and 3.3 h for APTS and BTSPA grafted samples, respectively (Eq. 2) (Table 5):

$$Y = kt \quad (2)$$

and $n = 0$ for $t \geq t^*$ (Eq. (3))

$$Y = 100 \quad (3)$$

As can be seen above, the diffusional release of the two molecules, R6G and ibuprofen, from the functionalized materials follows different mechanisms. This may have to do with the fact that the interaction of R6G with the organic functional groups is dominated by hydrophobic interaction while the interaction between ibuprofen and the organoamine and residual silanol groups of the functionalized mesoporous materials is dominated by hydrogen bonding. Suh et al. [23b] reported that the control of the inclusion and release characteristics of drug molecules in mesoporous materials by manipulating the molecular interactions such as hydrogen bonding between the host and guest molecules is possible. Although our FT-IR spectra (Fig. S4) did not conclusively reveal any possible such interaction and while Suh et al. [23b] have also not performed such an experiment, we believe that similar interactions as proposed by Suh et al. [23b] may have also played roles in the differences in adsorption capacity and release properties among our materials. In another report by Vallet-Regí and co-workers [13], not only the functional groups but also the loading of drug or the drug:host ratio is reported to also play an important role for drug release kinetics. Interestingly, the drug release profiles of our samples seem to show unusually slower drug release followed by faster release.

This kind of release profile is peculiar and, to our best knowledge, has never been reported for mesoporous materials. However, we do not know its underlying mechanism, which may warrant further investigations.

4. Conclusion

The adsorption capacity and release properties of mesoporous materials for different drug molecules can be improved by functionalizing them with judiciously chosen organic groups. Rhodamine 6G and ibuprofen, which have different structures and surface properties, were used as model drug molecules to conduct comparative adsorption and release studies of organic functionalized mesoporous materials that were synthesized by post-grafting and co-condensation. While mesoporous samples functionalized with mercaptopropyl and vinyl groups showed improved adsorption capacity for rhodamine 6G, samples functionalized with primary and secondary amine groups that were synthesized by grafting and co-condensation methods exhibited less adsorption capacity for rhodamine 6G. On the other hand, the trend in the degree of adsorption of ibuprofen was found to be the reverse of the results obtained for rhodamine 6G. The samples containing mercaptopropyl and vinyl groups showed less adsorption capacity for ibuprofen than the samples functionalized with primary and secondary amine groups. The release of the adsorbed molecules was also found to be dependent on the type of functional groups in the materials. The method of tuning adsorption capacity and release properties by organic functionalization of mesoporous materials could be extended to other organic functional groups and to a variety of other drug molecules. The resulting functionalized mesoporous materials may help to deliver drugs efficiently and, thus, minimize the drugs' possible adverse effects. Introducing secondary bioactive groups onto the external surface of the materials may also allow targeted delivery of the drug cargo to specific cells.

Acknowledgments

We gratefully acknowledge the partial financial support by the US National Science Foundation (NSF), CAREER Grant, CHE-0645348 for this work. EAB and ANO were partly supported by NSF-REU (Research Experiences for Undergraduates) program over Summer 2006 and 2007, respectively.

Appendix A. Supplementary material

Supplementary data associated with this article can be found in the online version at doi:10.1016/j.jssc.2009.03.034.

References

[1] [a] M. De, P.S. Ghosh, V.M. Rotello, Adv. Mater. 20 (2008) 1–17;
[b] P. Kolhe, E. Misra, R.M. Kannan, S. Kannan, M. Lieh-Lai, Int. J. Pharm. 259 (2003) 143–160.
[2] [a] C.T. Kresge, M.E. Leonowicz, W.J. Roth, J.C. Vartuli, J.S. Beck, Nature 359 (1992) 710–712;
[b] J.S. Beck, J.C. Vartuli, W.J. Roth, M.E. Leonowicz, C.T. Kresge, K.D. Schmitt, C.T.W. Chu, D.H. Olson, E.W. Sheppard, S.B. McCullen, J.B. Higgins, J.C. Schlenker, J. Am. Chem. Soc. 114 (1992) 10834–10843.
[3] [a] T. Yanagisawa, T. Shimizu, K. Kuroda, C. Kato, Bull. Chem. Soc. Jpn. 63 (1990) 1535–1537;
[b] S. Inagaki, Y. Fukushima, K. Kuroda, J. Chem. Soc., Chem. Commun. (1993) 680–682.
[4] [a] M. Vallet-Regi, A. Rámila, R.P. del Real, J. Pérez-Pariente, Chem. Mater. 13 (2001) 308–311;
[b] S.P. Rigby, M. Fairhead, C.F. van der Walle, Curr. Pharm. Des. 14 (2008) 1821–1831;
[c] I.I. Slowing, B.G. Trewyn, S. Giri, V.S.-Y. Lin, Adv. Funct. Mater. 17 (2007) 1225–1236;
[d] B.G. Trewyn, I.I. Slowing, S. Giri, H.-T. Chen, V.S.-Y. Lin, Acc. Chem. Res. 40 (2007) 846–853;
[e] F. Balas, M. Manzano, P. Horcajada, M. Vallet-Regí, J. Am. Chem. Soc. 128 (2006) 8116–8117;
[f] P. Horcajada, A. Rámila, G. Ferey, M. Vallet-Regí, Solid State Sci. 8 (2006) 1243–1249.
[5] [a] Z.G. Feng, Y.S. Li, D.C. Niu, L. Li, W. Zhao, H. Chen, L. Li, J. Gao, M. Ruan, J. Shi, Chem. Commun. (2008) 2629–2631;
[b] A. Sayari, S. Hamoudi, Chem. Mater. 13 (2001) 3151–3168.
[6] [a] A. Stein, B.J. Melde, R.C. Schroden, Adv. Mater. 12 (2000) 1403–1419;
[b] D. Brunel, A.C. Blanc, A. Galarneau, F. Fajula, Catal. Today 73 (2002) 139–152;
[c] J. Liu, X.-D. Feng, G.E. Fryxell, L.-Q. Wang, A.-Y. Kim, M.L. Gong, Adv. Mater. 10 (1998) 161–165;
[d] S. Shylesh, A.P. Singh, J. Catal. 244 (2006) 52–64.
[7] R. Mellaerts, J.A.G. Jammaer, M. Van Speybroeck, H. Chen, J. Van Humbeeck, P. Augustijns, G. Van den Mooter, J.A. Martens, Langmuir 24 (2008) 8651–8659.
[8] [a] S.P. Hudson, R.F. Padera, R. Langer, D.S. Kohane, Biomaterials 29 (2008) 4045–4055;
[b] R. Mellaerts, R. Mols, J.A.G. Jammaer, C.A. Aerts, P. Annaert, J.V. Humbeeck, G. Van den Mooter, P. Augustijns, J.A. Martens, Eur. J. Pharm. Biopharm. 69 (2008) 223–230.
[9] [a] J.M. Rosenholm, A. Meinander, E. Peuhu, R. Niemi, J.E. Eriksson, C. Sahlgren, M. Lindén, ACS Nano 3 (2009) 197–206;
[b] S.R. Blumen, K. Cheng, M.E. Ramos-Nino, D.J. Taatjes, D.J. Weiss, C.C. Landry, B.T. Mossman, Am. J. Respir. Cell Mol. 36 (2007) 333–342.
[10] [a] A. Rámila, B. Muñoz, J. Pérez-Pariente, M. Vallet-Regí, J. Sol–gel Sci. Technol. 26 (2003) 1199–1202;
[b] M. Vallet-Regi, J.C. Doadrio, A.L. Doadrio, I. Izquierdo-Barba, J. Perez-Pariente, Solid State Ionics 172 (2004) 435–439.
[11] [a] Y.F. Zhu, J.L. Shi, W.H. Shen, X.P. Dong, J.W. Feng, M.L. Ruan, Y.S. Li, Angew. Chem. Int. Ed. 44 (2005) 5083–5087;
[b] Y.-F. Zhu, J.-L. Shi, Y.-S. Li, H.-R. Chen, W.-H. Shen, X.-P. Dong, J. Mater. Res. 20 (2005) 54–61;
[c] Q. Yang, S.C. Wang, P.W. Fan, L.F. Wang, Y. Di, K.F. Lin, F.S. Xiao, Chem. Mater. 17 (2005) 5999–6003.
[12] [a] C.D. Nunes, P.D. Vaz, A.C. Fernandes, P. Ferreira, C.C. Romão, M.J. Calhorda, Eur. J. Pharm. Biopharm. 66 (2007) 357–365;
[b] Q.L. Tang, Y. Xu, D. Wu, Y.H. Sun, J. Solid State Chem. 179 (2006) 1513–1520;
[c] V. Ambrogi, L. Perioli, F. Marmottini, S. Giovagnoli, M. Esposito, C. Rossi, Eur. J. Pharm. Biopharm. 32 (2007) 216–222.
[13] [a] M. Vallet-Regí, F. Balas, D. Arcos, Angew. Chem. Int. Ed. 46 (2007) 7548–7558;
[b] R. Mellaerts, C.A. Aerts, J.V. Humbeeck, P. Augustijns, G.V. Mooter, J.A. Martens, Chem. Commun. 13 (2007) 1375–1377.
[14] F. Qu, G. Zhu, S. Huang, S. Li, J. Sun, D. Zhang, S. Qiu, Microporous Mesoporous Mater. 92 (2006) 1–9.
[15] [a] S.-W. Song, K. Hidajat, S. Kawi, Langmuir 21 (2005) 9568–9575;
[b] B. González, M. Colilla, M. Vallet-Regi, Chem. Mater. 20 (2008) 4826–4834.
[16] [a] T. Kokubo, H. Kushitani, S. Sakka, T. Kitsugi, T. Yamamuro, J. Biomed. Mater. Res. 24 (1990) 721–734;
[b] Q. Tang, Y. Xu, D. Wu, Y. Sun, J. Solid State Chem. 179 (2006) 1513–1520.
[17] K.K. Sharma, T. Asefa, Angew Chem. Int. Ed. 46 (2007) 2879–2882.
[18] [a] I.I. Slowing, B.G. Trewyn, S. Giri, V.S.-Y. Lin, Adv. Funct. Mater. 17 (2007) 1225–1236;
[b] B.G. Trewyn, I.I. Slowing, S. Giri, H.-T. Chen, V.S.-Y. Lin, Acc. Chem. Res. 40 (2007) 846–853;
[c] I.I. Slowing, J.-L. Vivero-Escoto, C.-W. Wu, V.S-Y. Lin, Adv. Drug Delivery Rev. 60 (2008) 1278–1288;
[d] S. Giri, B.G. Trewyn, V.S.-Y. Lin, Nanomedicine 2 (2007) 99–111.
[19] [a] F.Y. Qu, G.S. Zhu, S.Y. Huang, S.G. Li, J.Y. Sun, D.L. Zhang, S.L. Qiu, Microporous Mesoporous Mater. 92 (2006) 1;
[b] H. Vallhov, S. Gabrielsson, M. Stromme, A. Scheynius, A.E. Garcia-Bennett, Nano Lett. 7 (2007) 3576.
[20] [a] K.K. Sharma, T. Asefa, Angew. Chem. Int. Ed. 46 (2007) 2879–2882;
[b] K. Moller, T. Bein, Chem. Mater. 10 (1998) 2950–2963;
[c] G.E. Fryxell, J. Liu, T.A. Hauser, Z. Nie, K.F. Ferris, S. Mattigod, G. Meiling, R.T. Hallen, Chem. Mater. 11 (1999) 2148–2154.
[21] [a] J.A. Melero, R. van Grieken, G. Morales, Chem. Rev. 106 (2006) 3790–3812;
[b] M.H. Lim, C.F. Blanford, A. Stein, J. Am. Chem. Soc. 119 (1997) 4090–4091;
[c] M. Kruk, T. Asefa, M. Jaroniec, G.A. Ozin, Stud. Surf. Sci. Catal. 141 (2002) 197–204;
[d] I. Slowing, B.G. Trewyn, V.S.-Y. Lin, J. Am. Chem. Soc. 128 (2006) 14792–14793.
[22] S. Huh, J.W. Wiench, J.-C. Yoo, M. Pruski, V.S.-Y. Lin, Chem. Mater. 15 (2003) 4247–4256.
[23] [a] Y. Cho, R. Shi, R.B. Borgens, A. Ivanisevic, Nanomedicine 3 (2008) 507–519;
[b] M. Suh, H.-J. Lee, J.-Y. Park, U.-H. Lee, Y.-U. Kwon, D.J. Kim, Chem. Phys. Chem. 9 (2008) 1402–1408;

[c] B. Munoz, A. Ramila, J. Perez-Pariente, I. Diaz, M. Vallet-Regí, Chem. Mater. 15 (2003) 500–503;
[d] S.-W. Song, K. Hidajat, S. Kawi, Langmuir 21 (2005) 9568–9957;
[e] I. Izquierdo-Barba, A. Martinez, A.L. Doadrio, J. Pérez-Pariente, M. Vallet-Regí, Eur. J. Pharm. Biopharm. 26 (2005) 365–373;
[f] T. Sekine, K. Nakatani, Langmuir 18 (2002) 694–697;
[g] J.C. Doadrio, E.M.B. Sousa, I. Izquierdo-Barba, A.L. Doadrio, J. Perez-Pariente, M. Vallet-Regí, J. Mater. Chem. 16 (2006) 462–466.
[24] [a] K. Patel, S. Angelos, W.R. Dichtel, A. Coskun, Y.-W. Yang, J.I. Zink, J.F. Stoddart, J. Am. Chem. Soc. 130 (2008) 2382–2383;
[b] F. Qu, G. Zhu, H. Lin, J. Sun, D. Zhang, S. Li, S. Qiu, Eur. J. Inorg. Chem. (2006) 3943–3947;
[c] P. Yang, S. Huang, D. Kong, J. Lin, H. Fu, Inorg. Chem. 46 (2007) 3203–3211;
[d] M. Vallet-Regí, A. Ramila, R.P. Real, J. Perez-Pariente, Chem. Mater. 13 (2001) 308–311;
[e] Y.F. Zhu, J.L. Shi, Y.S. Li, H.R. Chen, W.H. Shen, X.P. Dong, Microporous Mesoporous Mater. 85 (2005) 75–81;
[f] T. Heikkilä, J. Salonen, J. Tuura, M.S. Hamdy, G. Mul, N. Kumar, T. Salmi, D.Y. Murzin, L. Laitinen, A.M. Kaukonen, Int. J. Pharm. 331 (2007) 133–138;
[g] C. Charnay, S. Bégu, C. Tourné-Péteilh, L. Nicole, D.A. Lerner, J.M. Devoisselle, Eur. J. Pharm. Biopharm. 57 (2004) 533–540.
[25] [a] U. Brohede, R. Atluri, A.E. Garcia-Bennett, M. Stromme, Curr. Drug Delivery 5 (2008) 177–185;
[b] Y.-Z. You, K.K. Kalebaila, S.L. Brock, D. Oupicky, Chem. Mater. 20 (2008) 3354–3359;
[c] H.Y. Huang, C.L. Yang, H. Zhang, M. Liu, Microporous Mesoporous Mater. 111 (2008) 254–259;
[d] S. Shen, P.S. Chow, S. Pui, S. Kim, K. Zhu, R.B.H. Tan, J. Colloid Interface Sci. 321 (2008) 365–372;
[e] J. Lu, E. Choi, F. Tamanoi, J.L. Zink, Small 4 (2008) 421–426.
[26] S. Sadhasivam, S. Savitha, K. Swaminathan, J. Environ. Manag. 85 (2007) 155–161.
[27] K.D. Rainsford, Ibuprofen, A Critical Biographical Review, CRC Press, Philadelphia, PA, 1999.
[28] A. Mehdi, C. Reyé, S. Brandés, R. Guilard, R.J.P. Corriu, New J. Chem. 29 (2005) 965–968.
[29] F. Qu, G. Zhu, S. Huang, S. Li, J. Sun, D. Zhang, S. Qiu, Microporous Mesoporous Mater. 92 (2006) 1.
[30] H. Vallhov, S. Gabrielsson, M. Stromme, A. Scheynius, A.E. Garcia-Bennett, Nano Lett. 7 (2007) 3576–3582.
[31] [a] M. Kruk, M. Jaroniec, Chem. Mater. 13 (2001) 3169–3183;
[b] K. Fodor, J.H. Bitter, K.P. de Jong, Microporous Mesoporous Mater. 56 (2002) 101–109;
[c] M. Kruk, M. Jaroniec, Chem. Mater. 12 (2000) 222–230.
[32] [a] M. Kruk, T. Asefa, M. Jaroniec, G.A. Ozin, J. Mater. Chem. 12 (2002) 3452–3457;
[b] L. Pasqua, F. Testa, R. Aiello, S. Cundari, J.B. Nagy, Microporous Mesoporous Mater. 103 (2007) 166–173.
[33] M.H. Lim, C.F. Blanford, A. Stein, Chem. Mater. 10 (1998) 467–470.
[34] [a] S. Zhu, Z. Zhou, D. Zhang, C. Jin, Z. Li, Microporous Mesoporous Mater. 106 (2007) 56–61;
[b] C.-Y. Hong, X. Li, C.-Y. Pan, J. Phys. Chem. C 112 (2008) 15320–15324;
[c] X. Yu, S. Ding, Z. Meng, Z. Yang, Colloid Polym. Sci. 286 (2008) 1361–1368;
[d] L. Zhang, J. Liu, J. Yang, Q. Yang, C. Li, Microporous Mesoporous Mater. 109 (2008) 172–183.
[35] M.V. Cagnoli, S.G. Casuscelli, A.M. Alvarez, J.F. Bengoa, N.G. Gallegos, M.E. Crivello, E.R. Herrero, S.G. Marchetti, Catal. Today 107–108 (2005) 397–403.
[36] A. Walcarius, M. Etienne, B. Lebeau, Chem. Mater. 15 (2003) 2161–2173.
[37] F. Qu, G. Zhu, H. Lin, J. Sun, D. Zhang, S. Li, S. Qiu, Eur. J. Inorg. Chem. 19 (2006) 3943–3947.
[38] P. Costa, J.M.S. Lobo, Eur. J. Pharm. 13 (2001) 123–133.
[39] T. Heikkilä, J. Salonen, J. Tuura, M.S. Hamdy, G. Mul, N. Kumar, T. Salmi, D.Y. Murzin, L. Laitinen, A.M. Kaukonen, J. Hirvonen, V.-P. Lehto, Int. J. Pharm. 331 (2007) 133–138.
[40] J. Andersson, J. Rosenholm, S. Areva, M. Lindén, Chem. Mater. 16 (2004) 4160–4167.